



Nanoscale Dynamics of Phase Flipping in Water near its Hypothesized Liquid-Liquid Critical Point

T. A. Kesselring¹, G. Franzese², S. V. Buldyrev³, H. J. Herrmann^{1,4} & H. E. Stanley⁵

¹Computational Physics, IfB, ETH Zurich, Schafmattstrasse 6, 8093 Zurich, Switzerland, ²Departament de Física Fonamental, Universitat de Barcelona, Diagonal 645, 08028 Barcelona, Spain, ³Department of Physics, Yeshiva University, 500 West 185th Street, New York, NY 10033, ⁴Departamento de Física, Universidade Federal do Ceará, Campus do Pici, 60451-970 Fortaleza, Ceará, Brazil, ⁵Center for Polymer Studies and Department of Physics, Boston University, Boston, MA 02215.

Received
2 April 2012

Accepted
30 May 2012

Published
29 June 2012

Correspondence and requests for materials should be addressed to T.A.K. (tobiaskesselring@ethz.ch)

One hypothesized explanation for water's anomalies imagines the existence of a liquid-liquid (LL) phase transition line separating two liquid phases and terminating at a LL critical point. We simulate the classic ST2 model of water for times up to 1000 ns and system size up to $N = 729$. We find that for state points near the LL transition line, the entire system flips rapidly between liquid states of high and low density. Our finite-size scaling analysis accurately locates both the LL transition line and its associated LL critical point. We test the stability of the two liquids with respect to the crystal and find that of the 350 systems simulated, only 3 of them crystallize and these 3 for the relatively small system size $N=343$ while for all other simulations the incipient crystallites vanish on a time scales smaller than ≈ 100 ns.

We perform extensive molecular dynamics (MD) simulations of ST2-water in the constant-temperature, constant-pressure ensemble. We equilibrate the system for ≈ 1000 ns for 127 state points in the supercooled liquid region of water. Pressure P ranges from 190 MPa to 240 MPa, while temperature T is as low as $T = 230$ K at high P , and 244 K at low P . We make 624 different simulations, 341 as long as 1000 ns, and for four system sizes, $N = 216$ (80 state points), 343 (75 state points), 512 (44 state points), and 729 molecules (46 state points). For the majority of state points studied we average our results over several (≤ 11) independent runs. We interpolate our data along isobars using the histogram reweighting method¹. For $P \gtrsim 200$ MPa, we find that the density ρ decreases sharply within a narrow temperature range, while at lower P it falls off with T continuously. This behavior is consistent with a discontinuous phase transition at high- P between a high-density liquid (HDL) and a low-density liquid (LDL) ending in a liquid-liquid (LL) critical point at lower P (Fig. 1a).

This LL critical point was hypothesized² based on studies of the ST2 model, and subsequently studied in detail by many others using, in addition to ST2^{3,4}, TIP5P⁵, TIP4P⁶, TIP4P-Ew⁷ and TIP4P/2005⁸ as well as coarse-grained models^{9–11}. The existence of the LL critical point allows one to understand X-ray spectroscopy results^{12–14,26}, and explains the increasing correlation length in bulk water upon cooling as found experimentally¹⁵ and the hysteresis effects¹⁶. Holten et al.^{17,18} reviews available experimental information and shows that the assumption of a LL critical point in supercooled water provides an accurate account on the experimental thermodynamic properties.

Abrupt changes in the global density ρ are related to the appearance of different local structures. Among various parameters describing the local structures we identify d_3 ¹⁹ and ψ_3 , defined in the Methods Section, as good quantities to distinguish the LDL and the HDL phase and the best quantities to distinguish them from ice. The average values of ψ_3 of the two phases differ by about 50%, the LDL phase being characterized by greater order in the second shell than in the HDL phase.

Liu et al.⁴, using histogram reweighted Monte Carlo methods in the grand canonical ensemble for only one but quite large system size, find an order parameter distribution function consistent with a critical point belonging to the universality class of a 3 dimensional (3d) Ising model. In Ref.31 Limmer and Chandler question this result using the umbrella sampling method to evaluate the free energy landscape of the ST2 model near a single state point and for a single system size ($N = 216$). They find two minima in the free energy landscape: one for liquids and one for crystalline structure. They do not find a third minimum corresponding to the LDL and conclude that the LDL does not exist as a metastable state, but only as a transitional state from HDL to crystal. However, Sciortino et al. in³³ show, with an implementation of the umbrella sampling with variable number of particles

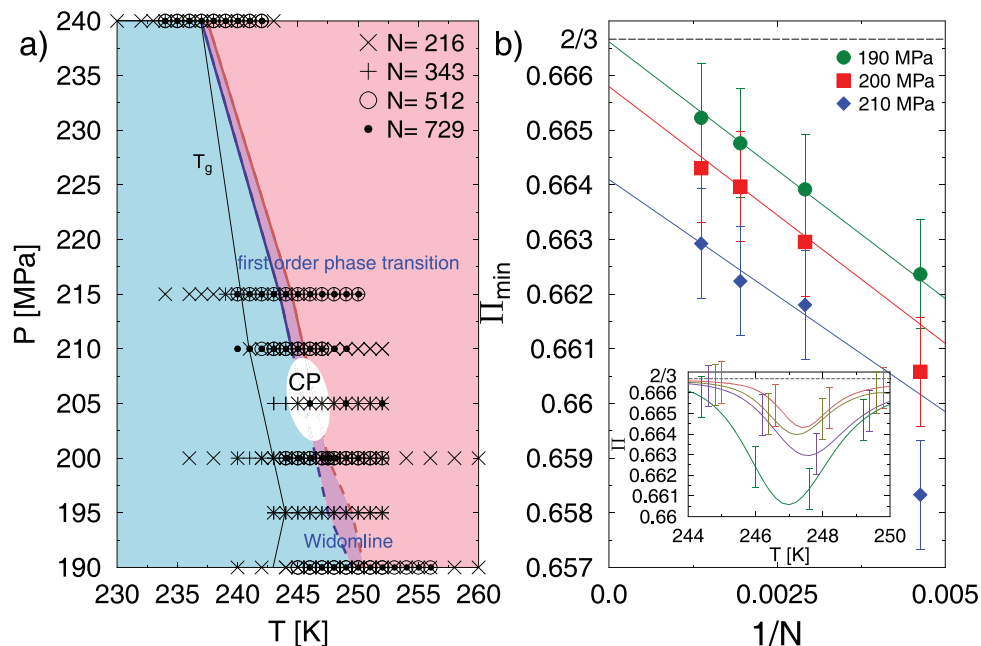


Figure 1 | Phase diagram and finite size scaling analysis to locate the line of liquid-liquid (LL) phase transitions. (a) State points in the P - T diagram simulated. Different symbols correspond to different sizes N . The high- T (red) region exhibits HDL-like states and the low- T (blue) region LDL-like states. In the intermediate (violet) region we observe flipping between HDL-like and LDL-like states. Below the black line T_g correlation times are larger than 100 ns, while above they are smaller and thus equilibrium is attained within reasonable simulation times. The white region, denoted CP, is our estimate of the location of the LL critical point in the thermodynamic limit. (b) Finite-size analysis of Π_{\min} along isobars crossing the discontinuous LL phase transition (violet at high P in (a)) and the Widom line (within the violet region at low P in (a)). At $P = 190$ MPa, Π_{\min} approaches $2/3$ when $N \rightarrow \infty$, indicating that the density distribution is unimodal and that one crosses the Widom line, and not the line of discontinuous phase transition. At $P = 200$ MPa, Π_{\min} approaches $\approx 2/3 - 0.001$, consistent within its error bar with the value expected at coexistence²⁰. At $P = 210$ MPa, Π_{\min} tends to a smaller value clearly excluding $2/3$ and therefore the distribution $\mathcal{D}(\rho)$ is bimodal, that is the fingerprint of a discontinuous LL phase transition. Π_{\min} depends linearly on $1/N$ to the leading order, displaying deviations only for the smallest size $N = 216$. The inset shows Π along the isobar at $P = 200$ MPa as a function of T for all four system sizes (from bottom to top: $N = 216, 343, 512, 729$) displaying a clear minimum Π_{\min} . Lines are interpolations obtained using histogram reweighting for up to eleven independent simulations of length 1000 ns.

$200 \leq N \leq 327$ of the umbrella sampling that guarantees very high resolution in the exploration of the free energy landscape, the presence of the minimum corresponding to the LDL state metastable with respect to the crystal, reconfirming the results of Ref.4 and at variance with Ref.31, 32. To contribute to the discussion, we present here a finite size scaling analysis of results from extremely long ($1\mu\text{s}$) MD simulations. We find that 1) LDL is a genuine liquid state, metastable with respect to the crystal, 2) LDL and HDL are separated by a first-order phase transition line ending in a critical point, 3) Close to the LLCP, LDL has relaxation times of the order of 100 ns, which show that 1000 ns runs are sufficient to equilibrate LDL, 4) the results are robust with respect to the finite size scaling analysis and show that the LDL-HDL critical point belongs to the 3 dimensional Ising model.

Results

To show that the LL phase transition exists in the thermodynamic limit, we perform a finite-size analysis along isobars within the supercooled liquid region. For this purpose, we calculate the Challa-Landau-Binder parameter $\Pi \equiv 1 - \langle \rho^4 \rangle / 3 \langle \rho^2 \rangle^2$ for the bimodality of the density distribution function, $\mathcal{D}(\rho)$ ^{20,21}. When $\mathcal{D}(\rho)$ is unimodal, Π adopts the value $2/3$ in the thermodynamic limit $N \rightarrow \infty$, while $\Pi < 2/3$ when $\mathcal{D}(\rho)$ is bimodal, since two phases coexist (Fig. 1b).

However, for a finite system $\Pi < 2/3$ whenever $\mathcal{D}(\rho)$ deviates from a delta function. This occurs in the region of the phase diagram where, for a finite system, the isothermal compressibility, K_T , has a maximum, i.e., along a locus in the P - T plane that includes (i) the discontinuous (in the thermodynamic limit) phase transition at $P > P_c$, the LL critical pressure, (ii) the effective LL critical point at $P_c(N)$,

where the discontinuity vanishes, and (iii) a line for $P < P_c$ that emanates from the LL critical point into the supercritical region. Near P_c this line follows the locus of maxima of the correlation length, known as the Widom line²², and deviates from it at lower P ²³.

The finite-size behavior of Π allows us to distinguish whether an isobar is above or below P_c ^{20,21} (Fig. 1b). When isobars cross the Widom line ($P < P_c$), Π displays a minimum Π_{\min} (inset in Fig. 1b) that in leading order approaches $2/3$ linearly with $1/N$. When $\mathcal{D}(\rho)$ consists of two Gaussians of equal weight, i.e. at the coexistence line for $P \geq P_c$, Π_{\min} approaches, also linearly with $1/N$, another limiting value $\Pi \rightarrow 2/3 - (\rho_H^2 - \rho_L^2)^2 / [3(\rho_H^2 + \rho_L^2)^2]$ where $\rho_H = \rho_H(P)$ and $\rho_L = \rho_L(P)$ are the densities of the two coexisting phases²⁰. This limiting value progressively decreases as P increase above P_c since $\rho_H - \rho_L$ increases at coexistence as $(P - P_c)^\beta$, where $\beta \approx 0.3$ is the critical exponent of the 3d Ising universality class¹⁷.

To ensure that the system is in thermal equilibrium, we calculate the correlation time for the first maximum k_1 of the oxygen-oxygen intermediate scattering function $S_{OO}(k, t)$, as used in Refs.24 and 25 and defined in the Methods Section. While correlation times in the HDL phase are very short (≈ 0.01 ns), they become of the order of 100 ns in the LDL phase, implying that simulations of less than $1\mu\text{s}$ are likely affected by poor statistical sampling (Fig. 2). For temperatures above the line T_g in Fig. 1a, correlation times are smaller than 100 ns and we can equilibrate the system within our simulation time.

Figure 3a shows a typical example of a simulation near the critical point for $N = 343$ molecules at $P = 215$ MPa and $T = 244$ K. Here the system exhibits phase flipping between LDL and HDL, with the lifetime of each phase distributed from ≈ 20 ns to ≈ 300 ns. This nanoscale phase flipping results in a bimodal density distribution (Fig. 3b)

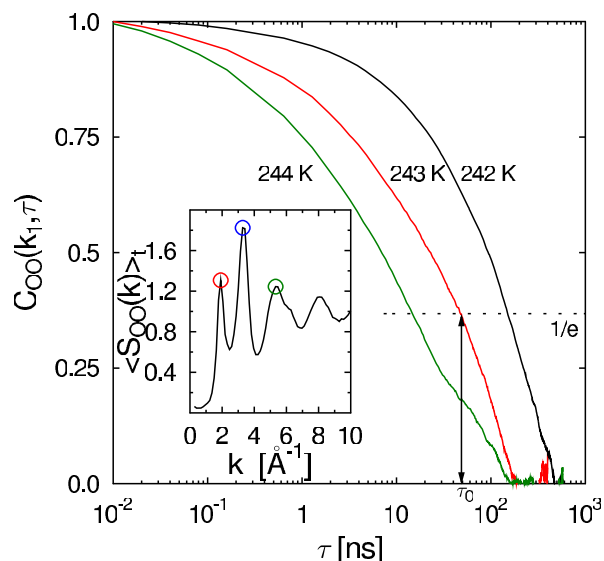


Figure 2 | Definition of the correlation time τ_0 using the intermediate scattering function. The correlation time τ_0 is calculated using the correlation function $C_{OO}(k, t)$ of the intermediate scattering function of the oxygen atoms $S_{OO}(k, t)$. For the k vectors corresponding to the first three maxima k_1, k_2 and k_3 (marked in red, blue and green in the inset), we calculate the evolution of the correlation function $C_{OO}(k_i, \tau)$. We then define the correlation time as the time for which $C_{OO}(k_i, \tau)$ decreases to $1/e$ for the slowest of the k_i vectors. For nearly all the state points k_1 has been the vector for which this decrease has been the slowest. We find $\tau = 10\text{--}100$ ns for the LDL phase, so we can equilibrate this phase in our simulations of about 1000 ns. Data are for a system of $N = 343$ molecules at pressure $P = 210$ MPa and temperatures (from left to right) $T = 244$ K, 243 K, in the LDL phase, and 242 K below the T_g line of Fig. 1a.

and is observed for all temperatures and pressures around the LL phase transition in a region that shrinks with growing system size.

Discussion

To estimate the critical exponents of the LL critical point we next investigate the distribution of the order parameter M of the LL phase transition. As for the liquid-gas phase transition²⁷, the order parameter is not simply the density, but a linear combination of the density with another observable²⁸. Here we choose the linear combination of density and energy $M \equiv \rho + sE^{27}$ and find that it follows, as expected, the behavior of a liquid in the universality class of the 3d Ising model, as is also the case for the liquid-gas transition (Fig. 4). At $P = 205$ MPa the difference between the maxima and the central minimum of the order parameter distribution is smaller than for the 3d Ising case. At $P = 210$ MPa it is larger and the critical point therefore seems to be in between, consistent with the conclusion obtained from the analysis of Π . We get the best fit of the order parameter distribution function at a pressure of $P = 206 \pm 3$ MPa and a temperature of $T = 246 \pm 1$ K.

The same analysis for $N = 512$ and 729 yields estimates, consistent with $N = 343$, of the LL critical point to be $P_c = 208 \pm 3$ MPa and $T_c = 246 \pm 1$ K (Fig. 4b, c). The finite size scaling of the amplitudes of the order parameter distribution $A \sim L^{\beta/\nu}$ is consistent with the behavior predicted for the 3d Ising universality class with $\beta/\nu \approx 0.518$ ²⁷ and strong corrections to scaling for $N \lesssim 343$ (Fig. 4d).

Finally, we investigate also the possibility of spontaneous crystal nucleation in the LDL phase using the structural order parameter d_3 ¹⁹. At temperatures below the region of phase flipping, the samples sometimes form large crystallites filling up to 10% of the system volume. Their structure exhibits a mixture of cubic and hexagonal symmetry. However, in approximately 99% of simulations these

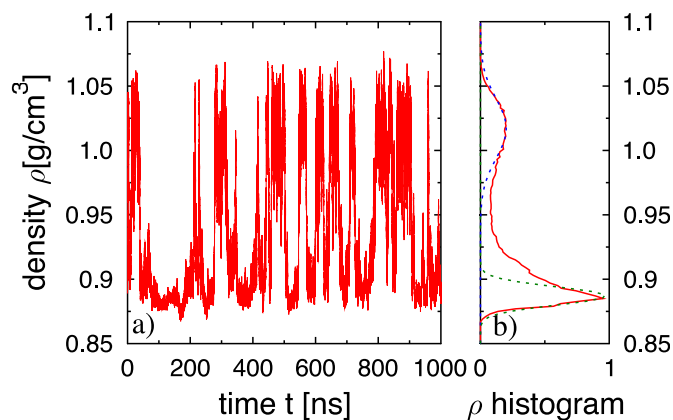


Figure 3 | Phase flipping between LDL and HDL at coexistence. (a) The 1 μ s time series shows how frequently, at constant $P = 215$ MPa and $T = 244$ K, $N = 343$ ST2-water molecules switch from LDL-like to HDL-like states. (b) The histogram for the sampled density values, in arbitrary units, after discarding the first 100 ns of the 1 μ s time series. For LDL-like states $\rho \approx (0.89 \pm 0.01)$ g/cm³ and for HDL-like states $\rho \approx (1.02 \pm 0.03)$ g/cm³ corresponding to a difference of $\approx 13\%$ in density. Dashed lines are Gaussian best fits of the histogram around the two maxima.

unstable crystallites vanish within the simulation time of 1000 ns, showing that the free-energy barrier for the crystallization process is significantly larger than $k_B T$ in the LDL phase (Fig. 5). We observe irreversible crystallization in only 3 out of 350 (1 μ s)-runs, for only $N = 343$ and all corresponding to state points near the LL critical point (Fig. 1a). This is consistent with the general result that a metastable fluid-fluid phase transition favors the crystallization process in its vicinity²⁹. We did not observe any crystallization events for $N = 512$ and $N = 729$ although the total simulation time for these systems is comparable to that of $N = 343$. The fact that the crystallization rate is not increasing with system size is evidence that LDL is the genuine metastable phase with respect to the stable crystal phase.

In conclusion, we use new methods to investigate both the statics and dynamics of deeply supercooled ST2-water. Specifically, we analyze static quantities (density and potential energy) using the framework of finite-size scaling theory, and we analyze the dynamic structure factor over three orders of magnitude of time scales, from 1 to 1000 ns. We find definitive evidence of a first order LL phase transition line between two genuine phases that are each metastable with respect to crystal. The phase transition line terminates in a LL critical point, and the exponents associated with this LL critical point are indistinguishable from those expected for a three-dimensional lattice-gas model which is used to describe the liquid-vapor critical point.

Methods

We performed MD simulations in the NPT ensemble using the Stillinger and Rahman³⁴ five-point water model ST2, consisting of five particles interacting through electrostatic and Lennard-Jones forces with a cutoff of 7.8 Å. The pressure was not adjusted to correct for the effects of the Lennard-Jones cutoff, since it would originate from mean field calculations, which become rather poor near a critical point.

We apply the *Shake* algorithm to constrain the particles inside each molecule. The constant pressure is imposed by a Berendsen barostat, and a Nosé-Hoover thermostat is applied to ensure constant temperature³⁵. Periodic boundary conditions have been implemented and reaction field method with a cutoff of 0.78 nm is used for the Coulomb's interactions.

For the simulations we used the following protocol consisting of three steps: (1) For any given density, a constant volume simulation is performed at $T = 300$ K during 1 ns (first pre-run). (2) The ensemble is then changed to NPT by adding the Berendsen barostat with the desired pressure and the temperature is reduced to $T = 265$ K, ensuring that the system reaches the HDL phase after 1 ns of equilibration (second pre-run). (3) After these two preruns the system is quenched to the desired temperature, from which the first 100–200 ns are removed as thermalization time. The choice of the thermalization time will be discussed next.

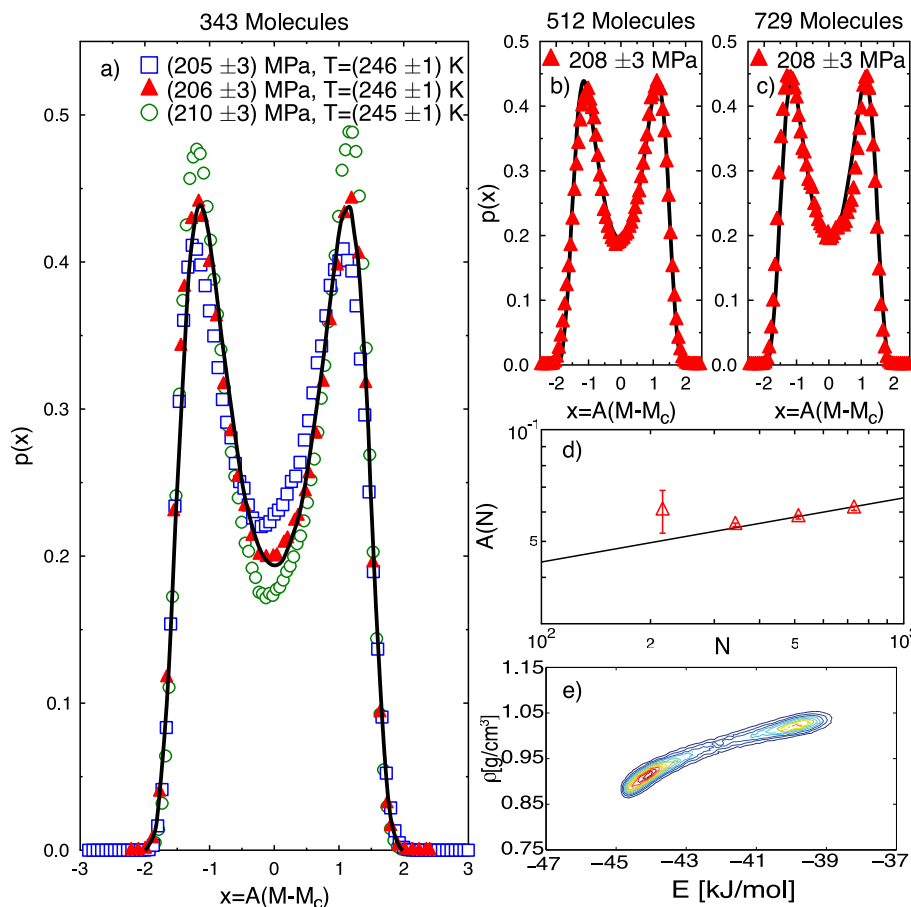


Figure 4 | The liquid-liquid critical point falls into the same universality class as the liquid-gas critical point. (a) The distribution function of the rescaled order parameter $x \equiv A(M - M_c)$ where $M \equiv \rho + sE$ with $s = 27.6 \frac{\text{g/cm}^3}{\text{kJ/mol}}$, follows for $P = (206 \pm 3)$ MPa and $T = (246 \pm 1)$ K (triangles) the order parameter distribution function of the 3d Ising model (solid line)³⁶. The data are from histogram reweighting of $N = 343$ molecules at $P = 205$ MPa and $T = 246.6$ K (squares), $P = 206$ MPa and $T = 246$ K (triangles) and $P = 210$ MPa and $T = 245.1$ K (circles). We repeat the analysis for (b) $N = 512$ and (c) $N = 729$. (d) For large sizes the amplitude A (triangles) scales as $A \sim L^{\beta/\nu}$, where $\beta/\nu \approx 0.52$, as in the 3d Ising universality class²⁷. For $N \lesssim 343$ corrections to scaling are strong. (e) Contour plot of the distribution of states in the density-energy plane, with red corresponding to the highest values and blue to the lowest. The distribution of the order parameter $M \equiv \rho + sE$ is obtained from this two-dimensional distribution by integrating it with a delta-function $\delta(M - \rho - sE)$. We select the value of s for which the distribution of M best fits the distribution of the order parameter for the 3d Ising universality class.

To decide whether the equilibration time is sufficient, we perform two steps. First, we inspect the time series of energy and density to discard the possibility of spontaneous crystallization. In all our NPT simulations we observed only three crystallization events ($\approx 1\%$ of total number of runs) all of them in systems with $N = 343$ molecules. We use them as a reference for the crystal. In a second step we measure the correlation time using the intermediate scattering function.

MD simulations are performed for a finite numbers of state points (Fig. 1a). We use the histogram reweighting method¹ to complement the statistics of each state point with the information from nearby state points. Histogram reweighting³⁰ is a method that combines the overlapping histograms of quantities calculated at close-enough state points, reweighting them with an appropriate factor that takes into account the difference in thermodynamic parameters. It is a powerful method that allows to calculate the observables for a continuous range of thermodynamic parameters within those directly simulated.

The order parameter $M \equiv \rho + sE$ is obtained from the distribution in the density-energy plane (Fig. 4e), by integrating it with a delta-function $\delta(M - \rho - sE)$. We select the value of s for which the distribution of M best fits the distribution of the order parameter for the 3d Ising universality class. The main effect found when changing s is a small shift in the estimated critical temperature T_c of about 0.1 K, which is less than the error of 0.5 K originating from the histogram reweighting.

The oxygen-oxygen intermediate scattering function $S_{OO}(\mathbf{k}, t)$ can be used to distinguish between phases of different structure, such as LDL and HDL. We also use it to estimate the correlation time. It is defined as

$$S_{OO}(\mathbf{k}, t) \equiv \frac{1}{N} \left\langle \sum_{\ell, m}^N \exp(ik \cdot [\mathbf{r}_\ell(t') - \mathbf{r}_m(t' + t)]) \right\rangle_{t'} \quad (1)$$

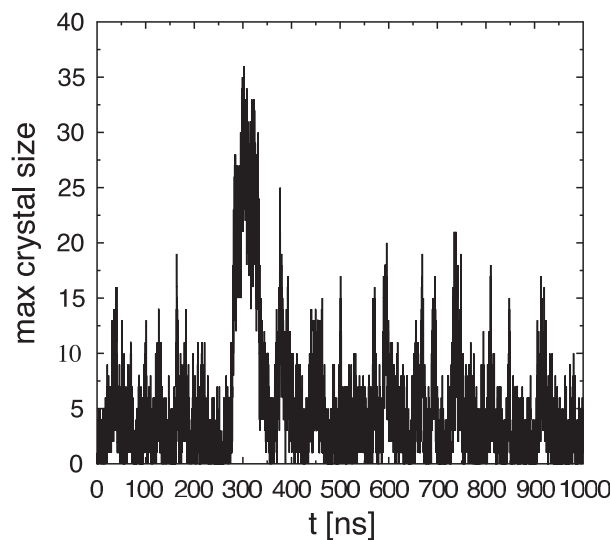


Figure 5 | Example of a simulation where the largest crystallite grows up to 35 molecules and then vanishes in a system having $N = 343$ molecules at a pressure of $P = 200$ MPa and $T = 246$ K. A molecule i is considered to belong to a crystal if $d_3(i, j) \leq d_c = -0.87$ for three out of its four bonds with nearest neighbors j .

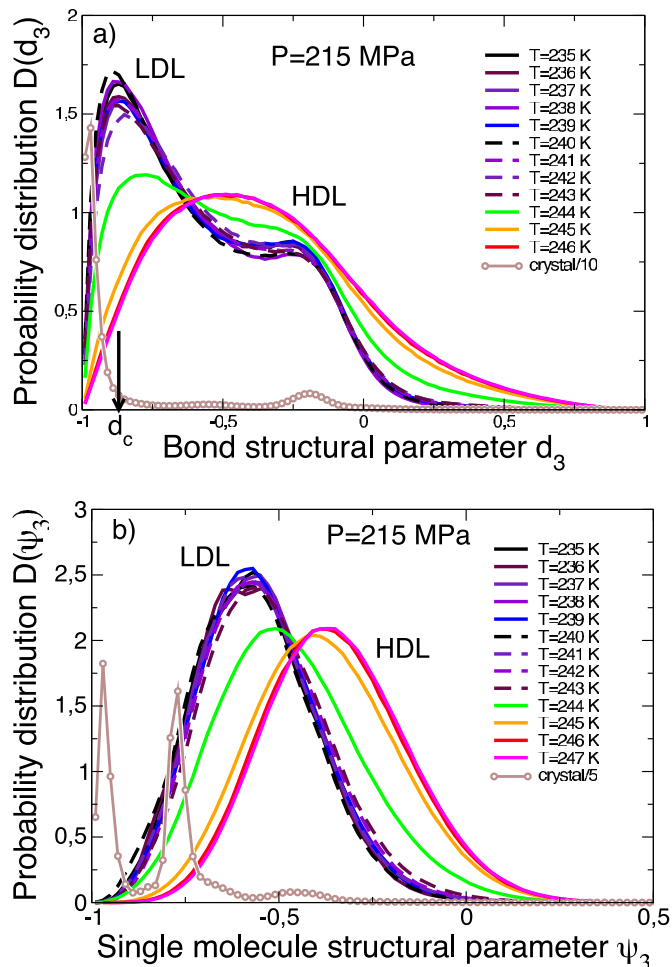


Figure 6 | The equilibrium probability distributions of two different structural parameters that allow us to distinguish among three structures: HDL, LDL, and crystal. (a) For the size of $N=343$, in the vicinity of the LL critical point in $\approx 1\%$ of the runs our system spontaneously crystallizes, forming structures with diamond and graphite patterns and with many defects. This structure is well characterized by the probability distribution $\mathcal{D}(d_3)$ (line with full dots) of the parameter d_3 , displaying a large maxima close to $d_3 = -1$, the value that corresponds to the perfect diamond crystal. Another small maximum at $d_3 = -1/9$ corresponds to the bonds connecting different layers in the graphite crystal. For the sake of comparison with the other cases, we divide $\mathcal{D}(d_3)$ of the crystal by 10. In the 99% of our simulations we find distributions $\mathcal{D}(d_3)$ as those presented here for $P = 215$ MPa, a pressure above the LL critical point pressure, and decreasing T (from right to left). $\mathcal{D}(d_3)$ shows an abrupt change when crossing the first-order LL phase transition region at $T \approx 244$ K. In particular, $\mathcal{D}(d_3)$ displays a pronounced shoulder at higher d_3 in the LDL phase, and is very different from the crystal case. The arrow marks the value $d_c = -0.87$ selected as two standard deviations from the peak of the crystal histogram corresponding to $d_3 = -1$ as in Ref.19. (b) The equilibrium probability distribution of the single-molecule parameter ψ_3 also distinguishes among HDL, LDL and crystal structures. The average values for fluid phases are $\psi_3 = -0.34 \pm 0.19$ in the HDL phase and $\psi_3 = -0.57 \pm 0.16$ in the LDL phase.

where $\langle \dots \rangle_t$ denotes averaging over the simulation time t' , $r_l(t')$ is the position vector of the oxygen of molecule l at time t' , \mathbf{k} is the wave vector and k is its magnitude $|\mathbf{k}|$. $S_{OO}(\mathbf{k}, t)$ describes the time evolution of the spatial correlation along the wave vector \mathbf{k} . Since the system has periodic boundaries, the components of \mathbf{k} have discrete values $2\pi j/L$, where L is the length of the simulation box and $j = 1, 2, \dots$. We define $S_{OO}(k, t) \equiv \langle S(\mathbf{k}, t) \rangle$, where average is taken over all vectors \mathbf{k} with magnitude k belonging to j th spherical bin $\pi(j-1/2)/L \leq k < \pi(j+1/2)/L$, for $j = 2, 3, \dots, 300$.

The temporal decay of $S_{OO}(k, t)$ is characterized by two relaxation times: (i) a short time, τ_β , after which $S_{OO}(k, t)$ reaches a plateau $S_{OO}(k, \tau_\beta)$ corresponding to the

bouncing of the particles inside the cages formed by their neighbors, and (ii) a long time, τ_α , corresponding to a particle escaping from its cage and diffusing away from its initial position. We define the correlation time $\tau = \tau_\alpha$ as the time for which $C_{OO}(k, \tau) \equiv S_{OO}(k, \tau)/S_{OO}(k, \tau_\beta) = 1/e$, where $C_{OO}(k, \tau)$ is the structural correlation function (Fig. 2).

We define the bond order parameter d_3 following Ref.19. The quantity $d_3(i, j)$ characterizes the bond between molecules i and j and is designed to distinguish between a fluid and a diamond structure. It uses the Y_3^m spherical harmonics to identify the tetrahedral symmetry of the diamond structure. In general, each molecule is characterized by a vector \mathbf{q}_i^j in the $(4\ell+2)$ -dimensional Euclidean space with components $\mathcal{R}e(q_{\ell, m}^i)$ and $\mathcal{I}m(q_{\ell, m}^i)$ ($m = -\ell, \dots, -1, 0, 1, \dots, \ell$), with

$$q_{\ell, m}^i \equiv \frac{1}{4} \sum_{j \in n_i} Y_\ell^m(\phi_{ij}, \vartheta_{ij}), \quad -\ell \leq m \leq \ell.$$

If molecule j belongs to the first coordination shell n_i (shell of four nearest neighbors) of molecule i , we define $d_3(i, j)$ as the cosine of the angle between two vectors \mathbf{q}_i^j and \mathbf{q}_j^i characterizing the first coordination shells of molecules j and i , respectively:

$$d_3(i, j) \equiv \frac{(\mathbf{q}_i^j \cdot \mathbf{q}_j^i)}{|\mathbf{q}_i^j| |\mathbf{q}_j^i|} \quad (2)$$

where

$$(\mathbf{q}_i^j \cdot \mathbf{q}_j^i) \equiv \sum_{m=-\ell}^{\ell} (\mathcal{R}e q_{\ell, m}^i \mathcal{R}e q_{\ell, m}^j + \mathcal{I}m q_{\ell, m}^i \mathcal{I}m q_{\ell, m}^j),$$

and $|\mathbf{q}_i^j| \equiv \sqrt{(\mathbf{q}_i^j \cdot \mathbf{q}_i^j)}$.

In a perfect diamond crystal $d_3(i, j) = -1$ for all bonds, while for a graphite crystal $d_3(i, j) = -1$ only for bonds connecting atoms in the same layer. For bonds connecting atoms in different layers $d_3(i, j) = -1/9$. Thus in graphite each atom has three out of four bonds having $d_3(i, j) = -1$. In our simulations, the spontaneously grown crystals have many defects, with different parts of the crystals following diamond or graphite patterns (Fig. 6a). Therefore, we consider a molecule in a crystal to have either three or four bonds with $d_3(i, j) < d_c = -0.87$, where the value of $d_c = -0.87$ is selected as two standard deviations from the peak of the crystal histogram corresponding to $d_3 = -1$. This is exactly the same criterion to specify molecules in the crystal state as in Ref.19. We find separate crystallites using the percolation criterion, i.e., two molecules satisfying the crystalline criterion belong to the same crystallite if they belong to the first coordination shell of each other (Fig. 5).

We finally observe that by defining $\psi_3(i) \equiv \frac{1}{4} \sum_{j=1}^4 d_3(i, j)$ as the average of d_3 over the four bonds of each molecule, we introduce a single-molecule structural parameter that also can be used to distinguish among the HDL, the LDL and the crystal phase (Fig. 6b).

- Panagiotopoulos, A. Z. Monte Carlo methods for phase equilibria of fluids. *J. Phys.: Condens. Matter* **12**, 25–52 (2000).
- Poole, P., Sciortino, F., Essmann, U. & Stanley, H. Phase-behavior of metastable water. *Nature* **360**, 324–328 (1992).
- Poole, P. H., Saika-Voivod, I. & Sciortino, F. Density minimum and liquid-liquid phase transition. *J. Phys.: Condens. Matter* **17**, L431–L437 (2005).
- Liu, Y., Panagiotopoulos, A. Z. & Debenedetti, P. G. Low-temperature fluid-phase behavior of ST2 water. *J. Chem. Phys.* **131**, 104508 (2009).
- Yamada, M., Mossa, S., Stanley, H. E. & Sciortino, F. Interplay between time-temperature-transformation and the liquid-liquid phase transition in water. *Phys. Rev. Lett.* **88**, 195701 (2002).
- Corradini, D., Rovere, M. & Gallo, P. A route to explain water anomalies from results on an aqueous solution of salt. *J. Chem. Phys.* **132**, 134508-1–134508-5 (2010).
- Paschek, D., Ruppert, A. & Geiger, A. Thermodynamic and structural characterization of the transformation from a metastable low-density to a very high-density form of supercooled TIP4P-Ew model water. *ChemPhysChem* **9**, 2737–2741 (2008).
- Abascal, J. L. F. & Vega, C. Widom line and the liquid-liquid critical point for the TIP4P/2005 water model. *J. Chem. Phys.* **133**, 234502 (2010).
- Franzese, G., Marqués, M. I. & Stanley, H. E. Intramolecular coupling as a mechanism for a liquid-liquid phase transition. *Phys. Rev. E* **67**, 011103 (2003).
- Franzese, G., Malescio, G., Skibinsky, A., Buldyrev, S. V. & Stanley, H. E. Generic mechanism for generating a liquid-liquid phase transition. *Nature* **409**, 692–695 (2001).
- Hsu, C. W., Largo, J., Sciortino, F. & Starr, F. W. Hierarchies of networked phases induced by multiple liquid-liquid critical points. *Proc Natl Acad Sci USA* **105**, 13711–13715 (2008).
- Nilsson, A. & Pettersson, L. G. M. Perspective on the structure of liquid water. *Chem. Phys.* **389**, 1–34 (2011).
- Wikfeldt, K. T., Nilsson, A. & Pettersson, L. G. M. Spatially inhomogeneous bimodal inherent structure of simulated liquid water. *Phys. Chem. Chem. Phys.* **13**, 19918–24 (2011).
- Tokushima, T. et al. High resolution X-ray emission spectroscopy of liquid water: The observation of two structural motifs. *Chemical Physics Letters* **460**, 387–400 (2008).



15. Huang, C. *et al.* Increasing correlation length in bulk supercooled H₂O, D₂O, and NaCl solution determined from small angle x-ray scattering. *J. Chem. Phys.* **133**, 134504 (2010).
16. Zhang, Y. *et al.* Density hysteresis of heavy water confined in a nanoporous silica matrix. *Proc Nat Acad Sci USA* **108**, 12206–12211 (2011).
17. Holten, V., Bertrand, C. E., Anisimov, M. A. & Sengers, J. V. Thermodynamics of supercooled water. *J. Chem. Phys.* **136**, 094507 (2012).
18. Holten, V., Kalová, J., Anisimov, M. A. & Sengers, J. V. Thermodynamics of liquid-liquid criticality in supercooled water in a mean-field approximation. *Int. J. Thermophys.* **10765**, 428–458 (2012).
19. Ghiringhelli, L. M. *et al.* State-of-the-art models for the phase diagram of carbon and diamond nucleation. *Mol. Phys.* **106**, 2011–2038 (2008).
20. Challa, M. S. S., Landau, D. P. & Binder, K. Finite-size effects at temperature-driven first-order transitions. *Phys. Rev. B* **34**, 1841–1852 (1986).
21. Franzese, G. Potts fully frustrated model: Thermodynamics, percolation, and dynamics in two dimensions. *Phys. Rev. E* **61**, 6383–6391 (2000).
22. Xu, L. *et al.* Relation between the Widom line and the dynamic crossover in systems with a liquid-liquid phase transition. *Proc Nat Acad Sci USA* **102**, 16558–16562 (2005).
23. Franzese, G. & Stanley, H. E. The Widom line of supercooled water. *J. Phys.: Condens. Matter* **19**, 205126 (2007).
24. Franzese, G., Malescio, G., Skibinsky, A., Buldyrev, S. V. & Stanley, H. E. Metastable liquid-liquid phase transition in a single-component system with only one crystal phase and no density anomaly. *Phys. Rev. E* **66**, 051206 (2002).
25. Starr, F. W., Sciortino, F. & H. E. Stanley, H. E. Dynamics of simulated water under pressure. *Phys. Rev. E* **60**, 6757–6768 (1999).
26. Huang, C. *et al.* The inhomogeneous structure of water at ambient conditions. *Proc. Nat. Acad. Sci. USA.* **106**, 15214–15218 (2009).
27. Wilding, N. B. Simulation studies of fluid critical behaviour. *J. Phys.: Condens. Matter* **585**, 585–612 (1997).
28. Bertrand, C. E. & Anisimov, M. A. Peculiar thermodynamics of the second critical point in supercooled water. *J. Phys. Chem. B* **115**, 14099–14112 (2011).
29. tenWolde, P. R. & Frenkel, D. Enhancement of protein crystal nucleation by critical density fluctuations. *Science* **277**, 1975–1978 (1997).
30. Ferrenberg, A. M. & Swendsen, R. H. Optimized Monte Carlo Data Analysis. *Phys. Ref. Lett.* **63**, 1195–1198 (1989).
31. Limmer, D. T. & Chandler, D. The putative liquid-liquid transition is a liquid-solid transition in atomistic models of water. *J. Chem. Phys.* **135**, 134503 (2011).
32. Poole, P. H., Becker, S. R., Sciortino, F. & Starr, F. W. Dynamical behavior near a liquid-liquid phase transition in simulations of supercooled water. *J. Phys. Chem. B* **115**, 14176–14183 (2011).
33. Sciortino, F., Saika-Voivod, I. & Poole, P. H. Study of the ST2 model of water close to the liquid-liquid critical point. *Phys. Chem. Chem. Phys.* **13**, 19759–64 (2011).
34. Stillinger, F. & Rahman, A. Improved simulation of liquid water by molecular-dynamics. *J. Chem. Phys.* **60**, 1545–1557 (1974).
35. Allen, M. P. & Tildesley, D. J. *Computer Simulation of Liquids*. Oxford Science Publications (Oxford University Press, 1987).
36. Hilfer, R. & Wilding, N. B. Are critical finite-size scaling functions calculable from knowledge of an appropriate critical exponent? *J. Phys. A: Math. Gen.* **28**, 281–286 (1995).

Acknowledgements

We thank Y. Liu, A. Z. Panagiotopoulos, P. Debenedetti, F. Sciortino, I. Saika-Voivod and P. H. Poole for sharing their results, obtained using approaches different from ours but also addressing the question of the hypothesized existence of a LL phase transition line and an associated LL critical point. We also thank S.-H. Chen, P. H. Poole, and F. Sciortino for a critical reading of the manuscript and for helpful suggestions. GF thanks Ministerio de Ciencia e Innovación-Fondo Europeo de Desarrollo Regional (Spain) Grant FIS2009-10210 for support. SVB acknowledges the partial support of this research through the Dr. Bernard W. Gamson Computational Science Center at Yeshiva College and through the Departament d'Universitats, Recerca i Societat de la Informació de la Generalitat de Catalunya. HES thanks the NSF Chemistry Division for support (grants CHE 0911389 and CHE 0908218).

Author contributions

T.K. performed the simulations. T.K., S.B. and G.F. evaluated the data. T.K., S.B., G.F., H.H. and E.S. wrote the paper. S.B., G.F., H.H. and E.S. supervised the project.

Additional information

Competing financial interests: The authors declare no competing financial interests.

License: This work is licensed under a Creative Commons Attribution-NonCommercial-ShareAlike 3.0 Unported License. To view a copy of this license, visit <http://creativecommons.org/licenses/by-nc-sa/3.0/>

How to cite this article: Kesselring, T.A., Franzese, G., Buldyrev, S.V., Herrmann, H.J. & Stanley, H.E. Nanoscale Dynamics of Phase Flipping in Water near its Hypothesized Liquid-Liquid Critical Point. *Sci. Rep.* **2**, 474; DOI:10.1038/srep00474 (2012).